UCRL-95853
PREPRINT

UCRL--95853

DE87 004360

REVIEW OF PROGRESS IN THE THEORY OF VOLUME PRODUCTION

J. R. HISKES

THIS PAPER WAS PREPARED FOR SUBMITTAL T.
FOURTH INTERNATIONAL SYMPOSIUM ON THE PRODU TION
AND NEUTRALIZATION OF NEGATIVE IONS AND BE S,
BROOKHAVEN NATIONAL LABORATORY
OCTOBER 27-31, 1986

OCTOBER 24, 1986

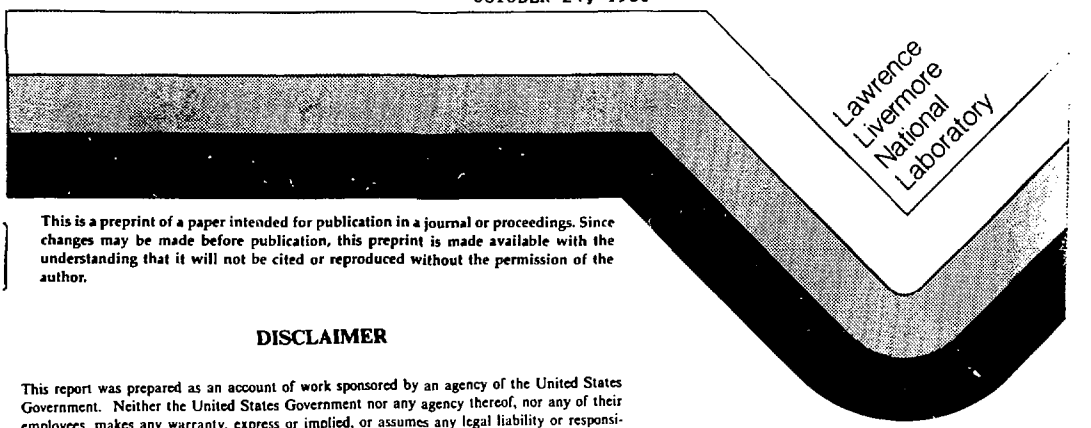

REVIEW OF PROGRESS IN THE THEORY OF VOLUME PRODUCTION*

J. R. Hiskes
Lawrence Livermore National Laboratory, University of California
Livermore, CA 94550

I. INTRODUCTION

With the demonstration[1] of large current densities extracted from hydrogen-discharge-type negative ion sources there has been a new emphasis directed toward the further development of these volume-type sources. Along with this emphasis has been a rapid increase in our understanding of the underlying atomic processes that occur in hydrogen-negative-ion discharges, together with a rapid evolution of the geometric configuration of these ion sources. An account of the development of the atomic processes in negative hydrogen discharges has been given in a recent review.[2] Here we shall emphasize these atomic developments as they bear on the tandem high-density ion-source configuration.

II. DISCUSSION

Figure 1 shows a schematic of a tandem negative ion generator in which vibrationally excited molecules are generated in chamber one and dissociative attachment to these molecules to form negative ions occurs in chamber two. The magnetic filter supports a

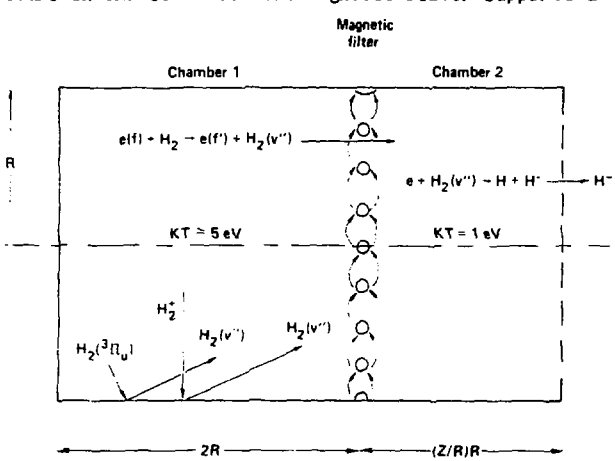

Figure 1. Schematic of a tandem negative ion generator.

*Work performed under the auspices of the U.S. Department of Energy by the Lawrence Livermore National Laboratory under contract number W-7405-ENG-48.

relatively large concentration of fast electrons, E > 25 eV, in chamber one while maintaining a low temperature, kT ~ 1 eV, thermal electron bath in the second chamber. In chamber one, three sources of vibrationally excited molecules, $H_2(v'')$, are shown: Auger relaxation of electronically excited $H_2(^3\Pi_u)$ molecules while undergoing wall collisions,[3] Auger neutralization of H_2^+ molecular ions during wall collisions,[4,5] and excitation by fast electrons through the excited electronic singlet states to provide residual vibrational excitation.[6-9] In different regimes each of these sources of vibrational excitation can predominate. At low electron densities, $n < 10^{11}$ cm^{-3}, and for discharge potentials below 30-40 eV the $^3\Pi_u$ relaxation will dominate.[3] For discharges rich in H_2^+ ions and operating at moderately low pressures the H_2^+ Auger neutralization can dominate.[10] But for most high density operation, $n > 10^{12}$ cm^{-3}, the singlet excitations will represent the principal source of vibrational excitation and it is these that we shall mainly be concerned with here.

As this system is optimized to provide the maximum extracted current density, the position along the axis of the second chamber, z/R, of the current density maximum shifts to smaller values of z/R as the first chamber and second chamber electron densities, n(1) and n(2), increase.[10] These increases in electron density increase the atomic number density and hence attenuate the vibrational excitation; the negative ions are also directly attenuated by associative detachment.[11,12] The optimum current density along the second chamber, as indicated in Fig. 2, is obtained at an axial position that is approximately equal to a mean free path beyond the filter against these collision processes. As the electron density in the two chambers is increased so as to enhance the negative ion yield, considerable emphasis must be placed on achieving the shortest possible length for the second chamber.

Leung et al.[13] have observed a variation of extraction current with second chamber length but at intermediate electron densities, $n \sim 10^{11}$ cm^{-3}. These densities are too small to generate a short mean free path for $H_2(v'')$ or H^- attenuation, and there is apparently an additional cause for second chamber attenuation. This may be related to a rapid falloff of underlying electron density in moving through the filter into the second chamber. To achieve the maximum negative ion current density, the requisite underlying electron density must be maintained as far as the extraction plane, i.e., up to the point of optimum negative ion concentration. Until the present time no source has operated at sufficiently high density to demonstrate an optimum second chamber length due to the collisional attenuation processes.

An experiment whose purpose is to rationalize the tandem concept has been performed[14] by injecting electrons of varying energy into the second chamber and identifying the different H^- formation processes by their respective energy dependences. The relative enhancement of H^- yield as a function of the difference of plasma potential and filament bias is shown in Fig. 3. The negative ion yield is seen to increase as the effective electron energy is decreased. This would seem to preclude the polar dissociation process, the reaction at the bottom of the figure, since its maximum rate is above 30 eV, and exhibits a threshold near 17 eV. The rise from 10 eV to 4 eV could possibly be due to the recombinational

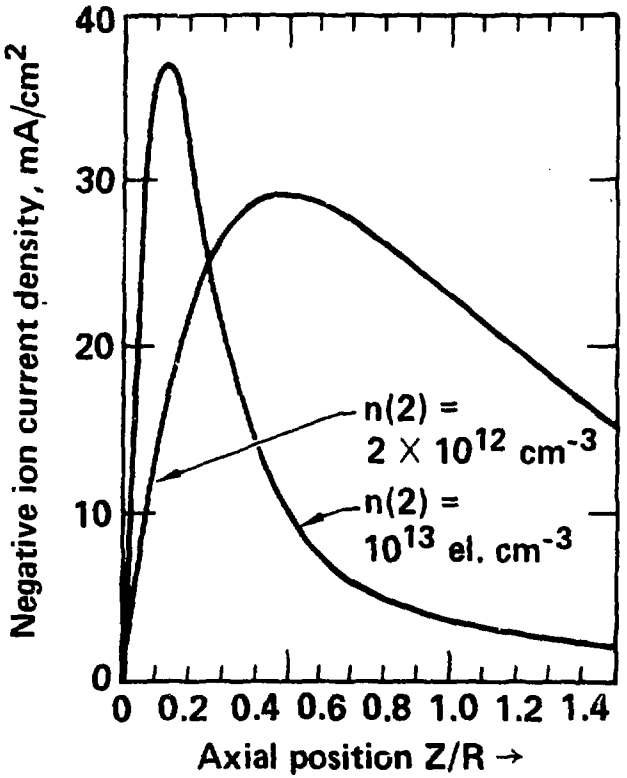

Figure 2. Current density along second chamber.

attachment of electrons to H_3^+ ions,[15] since this process has a maximum cross section in this energy range.[15] The maximum enhancement at the lowest energies, 0.5-1.0 eV, is consistent with either recombinational attachment of H_2 or dissociative attachment of $H_2(v")$.[16,17] If the apparent drop between 1.0 eV and 0.5 eV shown in the figure is not considered to be experimentally significant, the rise at low energies is consistent with H_2^+ recombinational attachment.[18] If the fall from 1.0 to 0.5 eV is taken at face value, the result is consistent only with $H_2(v")$ dissociative attachment.

Since the 1983 BNL Symposium, there has been some clarification of the first chamber optimization. At low densities the principal relaxation process of the vibrational excitation is wall collisions. But as the fast electron density increases, the electron collisional destruction of the vibrationally excited levels becomes the dominant loss of $H_2(v")$, and the active vibrational

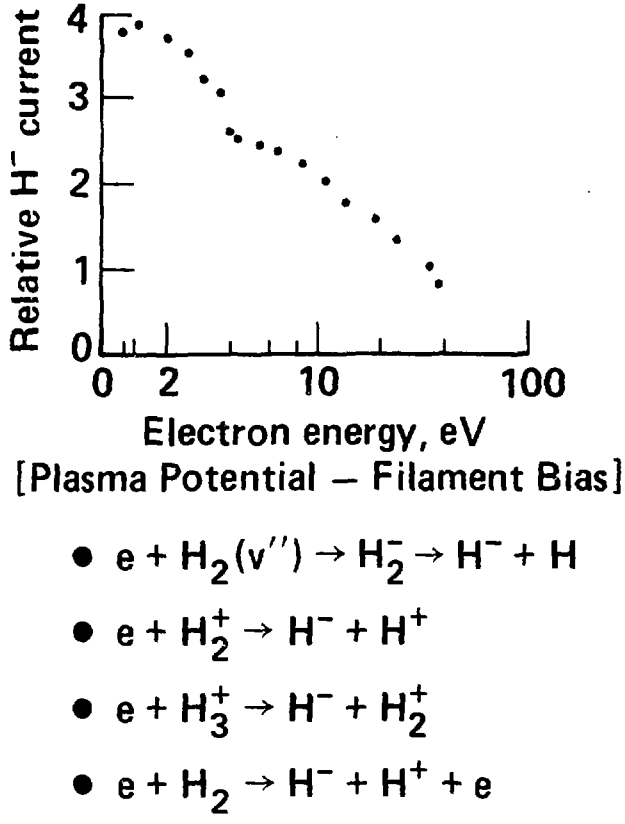

Figure 3. Current enhancement vs electron energy.

population approaches an asymptotic value.[19] This is illustrated in Fig. 4 for a system with scale length R = 10 cm and with a ratio of fast (E > 25 eV) to thermal electrons equal to one-tenth. Two solutions are shown: the solid curve for no atomic concentration and the dashed curve for an atomic concentration equal to the molecular concentration.

The performance of the second chamber depends both on the dissociative attachment process and the various loss processes. An extensive array of dissociative attachment cross sections as functions of vibrational and rotational quantum number have been prepared by Wadehra.[17] These calculations are based on a semi-empirical local-potential resonance model developed earlier by Wadehra and Bardsley[20] and fit to the experimental data of Allan and Wong.[16] An alternative model for dissociative attachment has been developed by Gauyacq.[21] In Gauyacq's model the transition is not imagined to proceed through a resonance state, but instead the

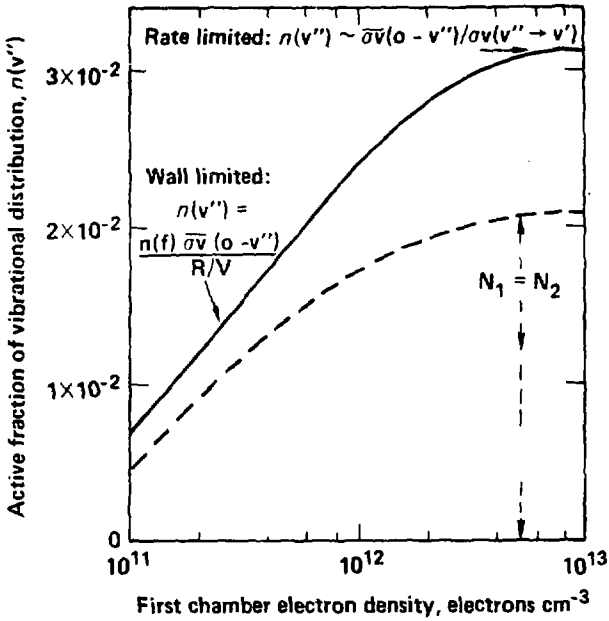

Figure 4. Vibrational population vs electron density.

vibrational excitation and electron capture are induced by the non-adiabatic electronic-vibration coupling terms. In this model a parameter is inserted to provide agreement with the Allen and Wong data up to v" = 4. One has in hand then two semi-empirical models for extrapolating the cross sections into the upper portion of the vibrational spectrum. A comparison of the cross section values for these two models is shown in Fig. 5. The Gauyacq values differ from those of Wadehra and Bardsley for levels v" = 5,6,7 by about 30 to 80%.

An attempt at an essentially exact calculation of dissociative attachment has been initiated by Mundel et al.[22] based upon a full nonlocal-potential resonance model. These calculations have been carried out for the v" = 0, 1, and 2 levels and fall below the experimental values of Allan and Wong. It would be most desirable to have these calculations extended into the upper portion of the spectrum.

In Fig. 6 is plotted the vibrational population distribution generated in chamber one for a high density discharge and the dissociative attachment rates that are appropriate to chamber two. The product of these rates, designated the negative-ion-source-function, is proportional to the negative ion production in the limit of a very short second chamber. This function is also shown in the figure. Inspection of the NISF shows that in excess of 90% of the total negative ion yield is derived from the middle portion of the vibrational spectrum, $5 \leq v'' \leq 11$.

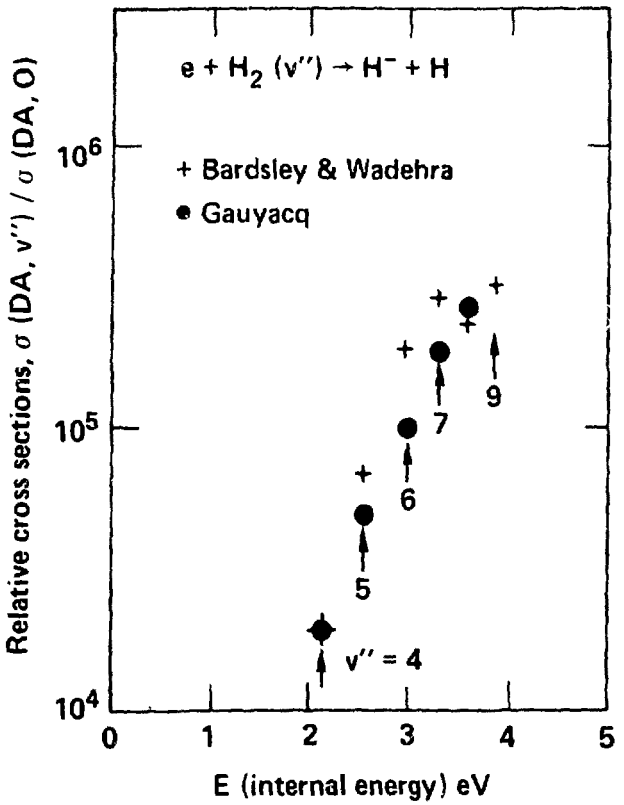

Figure 5. Comparison of dissociative attachment calculations.

The principal negative ion loss processes of concern in the second chamber are ion-ion neutralization,

$$H^- + H^+ \rightarrow H + H \quad , \tag{1}$$

and associative detachment[11,12]

$$H^- + H \rightarrow H_2(v'') + e \quad . \tag{2}$$

The theoretical and experimental activity with reference to reaction (1) is summarized in Fig. 7.[23-29] Only a brief summary statement of the situation is given here, the reader is referred to the references for an account of the new developments. At collision energies above about 10 eV, the current theoretical and experimental results are in fair agreement. At energies below 4 eV the two theoretical results, Refs. 23 and 29, are in agreement, but lie below the experimental data of Moseley et al.[24] At the collision

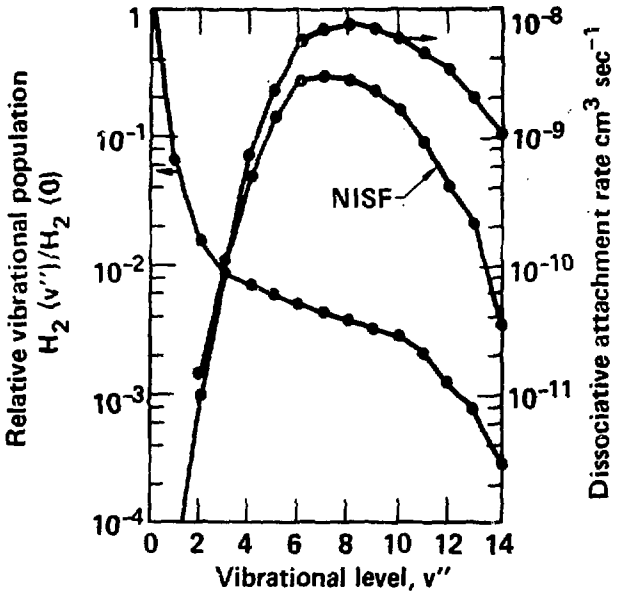

Figure 6. Negative ion source function vs vibrational level.

energy of interest to volume-type negative ion sources, energies near 1 eV, the theoretical cross sections are approximately a factor of three smaller than the experimental values.

With reference to the associative detachment process, reaction (2), the uncertainties are qualitatively different. Here the cross sections are not so uncertain, but very little is known of the concentration of H atoms. Among the greatest uncertainties in evaluating the potential performance of high-density negative ion sources is the almost complete lack of information concerning the atomic concentration.

The variation of negative ion density or current density along the length of the second chamber necessitates a spatial analysis of the ion density in this region. In the low-density, single-chamber discharge where mean free paths are long compared to system dimensions and negative ions are generated uniformly throughout the volume, a spatially independent density analysis will suffice. But in the second chamber of the tandem system a zero dimensional analysis will considerably overestimate the negative ion concentration. This is illustrated in Fig. 8. Here the solid curves are a reproduction of those of Fig. 2, and the upper dashed curve, calculated with a spatially-independent model, is to be compared with the lower solid curve. The spatially-independent model gives a negative ion current density that is almost three times larger than the peak value of the spatially-dependent model. The situation is emphasized further if there are a significant number of free atoms in the discharge. If $N_1 = N_2$ the spatially-dependent solution is reduced to that shown in the lower left-hand

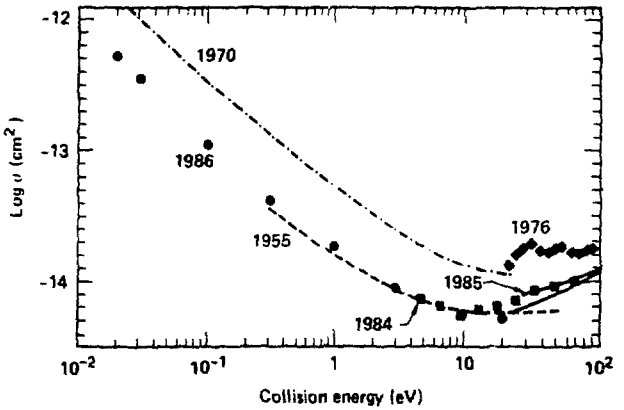

--- Bates & Lewis 1955
-·- Moseley et al. 1970
● Peart et al. 1976
—— Sidis et al. 1981
■ Szücs et al. 1984
----- Peart et al. 1985
● Fussen Kubach 1986

Figure 7. Neutralization cross sections.

corner. The spatially-independent solution is now some six times larger than the peak value.

The scaling law[19] for the tandem system allows one to judge the relative performance of different sources and provides a basis for extrapolating the performance of a particular source to higher current densities. The scaling law can be stated in either of two ways: If one has a particular source geometry with scale length R_0 providing a current density j_0, upon scaling all dimensions downward to a new scale factor R_b and increasing all densities by the factor R_0/R_b while holding the electron energy distribution fixed, the new current density will increase to $j_b = (R_0/R_b)\, j_0$. Alternatively, if one has optimized the current density j_0 of a system with scale length R_0, then the new optimized system with scale length R_b will emit a current density equal to $j_b = (R_0/R_b)\, j_0$.

These arguments can be applied to different systems, in a manner shown in Fig. 9. This figure is a plot of extracted current density vs scale length upon which is plotted the data points for three different ion source experiments.[1,30,31] Indicated on the figure is the second-chamber z/R value estimated from the geometry of these different sources. In the source of Holmes et al.[30] (HDG) 6 mA cm^{-2} are extracted from a 10 cm system. If this system were scaled downward to one centimeter the current density would scale up to 60 mA cm^{-2}. The ion source of Jimbo et al.[31] (JELP) is a small 1-cm Penning-type source from which has been extracted a current density of

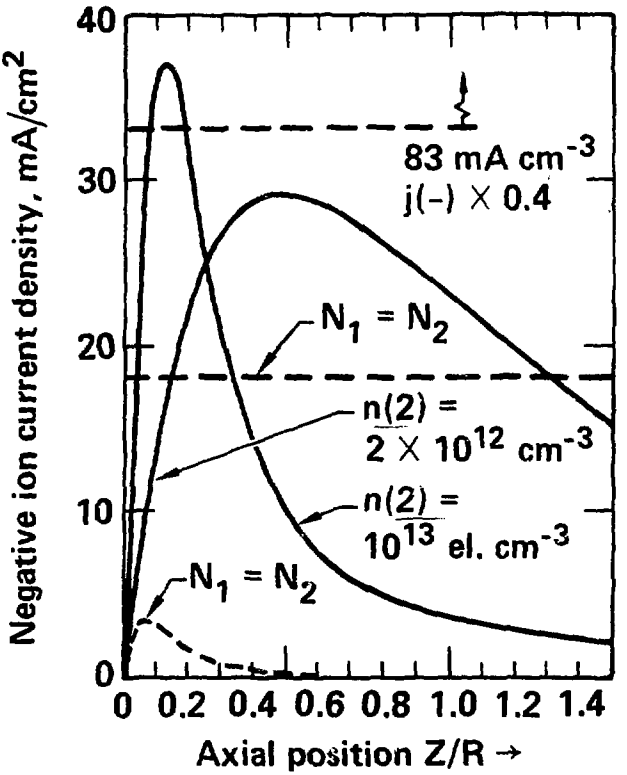

Figure 8. Current density along second chamber.

100 mA cm^{-2}. The ten centimeter source of York et al.[1] (YSLE) would scale to 370 mA cm^{-2} at one centimeter. This scaling tells us that the 100 mA cm^{-2} operation of the Penning source was not an optimized performance, but has the potential for almost a four-fold increase. The ten centimeter systems, Refs. 1 and 30, are known to be non-optimum since the extracted current density was still increasing for increasing discharge current; rather, the operation of these sources was power supply limited. Hiskes et al.[16] have projected an extracted current density of 60 to 80 mA cm^{-2} from a 10 cm system for an atomic concentration equal to one-tenth the molecular concentration; the specific value depending upon the ion drift velocity in the second chamber. This projected value would scale upwards to 600-800 mA cm^{-2} at the one centimeter scale. The high-density tandem system continues to have potential for large increases in the current density.

With the scaling of the current density established, the scaling of the other beam qualities, total current, emittance, and brightness follows immediately.[32] As an example of these scalings consider a cylindrical beam system of radius R_0 scaled downward to a

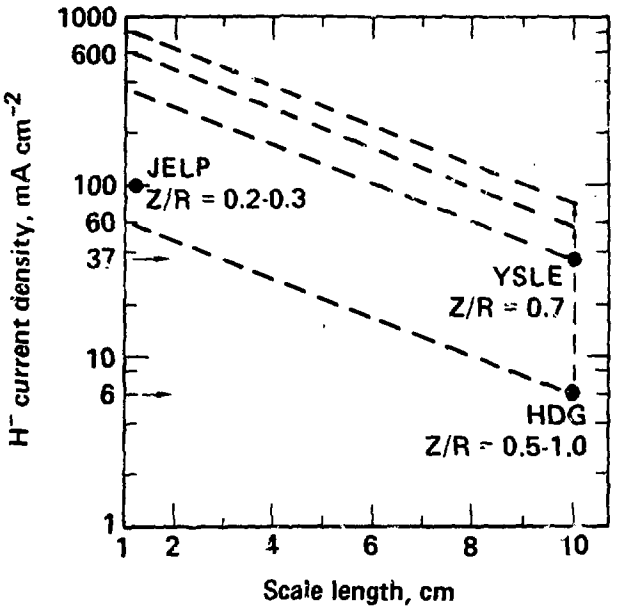

Figure 9. Current density vs scale length.

beamlet of radius R_b to give a beamlet current density $j_b = (R_0/R_b)\, j_0$. If several of these beamlets are now packed together to fill the original cylinder of radius R_0, one has effectively enhanced the new total current by the scale factor, $J_b = (R_0/R_b)\, J_0$. The emittance of the new system remains unchanged since the aperture and negative ion energies are unchanged. The source brightness, defined as the ratio of the total current to the square of the transverse emittance, also scales in proportion to R_0/R_b. These scalings are summarized in Fig. 10. The geometric scaling process provides for a favorable enhancement of the different beam qualities, current density, total current, and brightness while the emittance remains unchanged.

III. CONCLUSIONS

The concept of the tandem negative ion generator is now reasonably well defined. The cross section and rate processes for many of the principal underlying atomic and molecular processes are in hand, but certain excited molecular and negative ion destruction processes remain to be clarified. Experimental confirmation of the principal operative mechanisms in the first and second chambers are still largely lacking, notably the demonstration of suitable populations of vibrationally excited molecules in the first chamber, and the concentration of neutral atoms in the overall system and their affect upon the second chamber attenuation.

Current density:

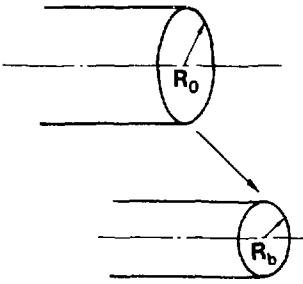

$j_0(-)$

$n(e) \sim 1/R_b,\ N_2 \sim 1/R_b$

$$j_b(-) = \frac{R_0}{R_b} j_0(-)$$

Total current:

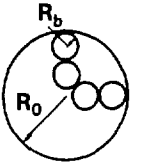

$$J_b = f \times \frac{j_b(-)}{j_0(-)} J_0 = f \frac{R_0}{R_b} J_0$$

Emittance: $\epsilon \sim R_0 \frac{dr}{dt}(-) \sim$ invariant

Brightness: $J_b/\epsilon^2 \sim j_b(-)/\left[\frac{dr}{dt}(-)\right]^2 \sim 1/R_b$

Figure 10. Summary of beam quality scalings.

The negative ion current densities that appear to be achievable in a tandem system with a scale length of 10 cm are only marginally interesting for application to neutral beams for magnetic fusion. The scaling of these sources to smaller dimensions will enhance the current density, but at the cost of higher source pressure and power density. The useful scaling that can be achieved represents a compromise between gas density and current density, but the full dimensions of this compromise remain to be clarified.

REFERENCES

1. R. L. York, R. R. Stevens, K. N. Leung, and K. W. Ehlers, Rev. Sci. Instrum. 55, 681 (1984).
2. J. R. Hiskes, Comments on Atomic and Molecular Physics, 19(2) (1987).
3. J. R. Hiskes and A. M. Karo, "Electron Energy Distributions, Vibrational Population Distributions, and Negative Ion Concentrations in Hydrogen Discharges," presented at the NATO Advanced Study Institute on Atomic and Molecular Processes in Contr. Thermo. Research, Palermo, Italy, July 19-30, 1982, Rept. No. UCRL-87779, June 1982.
4. J. R. Hiskes and A. M. Karo, AIP Conf. Proc. 111, 125 (1984).
5. A. M. Karo, J. R. Hiskes, and R. J. Hardy, J. Vac. Sci. Technol. A3(3), 1222 (1985).
6. J. R. Hiskes, J. Appl. Phys. 51(9), 4592 (1980).
7. J. M. Ajello, S. K. Srivastava, Y. L. Yung, Phys. Rev. A25, 2485 (1982).
8. W. G. Graham, J. Phys. D17, 2225 (1984).
9. J. Marx, A. Lebehot, and R. Campargue, J. Physique 46, 1667 (1985).
10. J. R. Hiskes, A. M. Karo, and P. A. Willmann, J. Vac. Sci. Technol. A3(3) 1229 (1985).
11. R. J. Bieniek and A. Dalgarno, Astroph. J. 228, 635 (1979).
12. R. J. Bieniek, J. Phys. B13, 4405 (1980).
13. K. N. Leung, K. W. Ehlers, and R. V. Pyle, Rev. Sci. Instr. 56, 364 (1985).
14. K. N. Leung, K. W. Ehlers, and R. V. Pyle, Rev. Sci. Instr. 57, 321 (1986).
15. B. Peart, R. A. Forrest, and K. Dolder, J. Phys. B12, 3441 (1979).
16. M. Allan and S. F. Wong, Phys. Rev. Lett. 41, 1795 (1978).
17. J. M. Wadehra, Phys. Rev. A29, 106 (1984).
18. B. Peart and K. T. Dolder, J. Phys. B8, 1570 (1975).
19. J. R. Hiskes, A. M. Karo, and P. A. Willmann, J. Appl. Phys. 58(5), 1759 (1985).
20. J. M. Wadehra and J. N. Bardsley, Phys. Rev. A20, 1398 (1979).
21. J. P. Gauyacq, J. Phys. B18, 1859 (1985).
22. C. Mundel, M. Berman, and W. Domcke, Phys. Rev. A32, 181 (1985).
23. D. R. Bates and J. T. Lewis, Proc. Phys. Soc. A68, 173 (1955).
24. J. T. Moseley, R. E. Olson, J. R. Peterson, Case Stud. At. Phys. 5, 1 (1975).
25. B. Peart, R. Grey, and K. Dolder, J. Phys. B9, L369 (1976).
26. V. Sidis, C. Kubach, and D. Fussen, Phys. Rev. Lett. 47, 1280 (1981).
27. S. Szucs, M. Karemera, M. Terao, and F. Brouillard, J. Phys. B17, 1613 (1984).
28. B. Peart, M. A. Bennet, and K. Dolder, J. Phys. B18, L439 (1985).
29. D. Fussen and C. Kubach, J. Phys. B19, L31 (1986).
30. A. J. T. Holmes, G. Dammertz, and T. S. Green, Rev. Sci. Instrum. 56(9), 1697 (1985).

31. K. Jimbo, K. W. Ehlers, K. N. Leung, and R. V. Pyle, Nucl. Instrum. and Methods A248, 282 (1986).
32. J. R. Hiskes, "Scaling of Current Density, Total Current, Emittance, and Brightness for Hydrogen Negative Ion Sources," Proc. of the NATO Advanced Study Institute on High Brightness Accelerators, Pitlochry, Scotland, July 13-25, 1986.

PQ612099/MM